Theoretical analysis of the microwave-drill near-field localized heating effect

E. Jerby,[a] O. Aktushev, and V. Dikhtyar
Faculty of Engineering, Tel Aviv University, Ramat Aviv 69978, Israel

(Received 9 August 2004; accepted 28 October 2004; published online 18 January 2005)

The microwave-drill principle [Jerby *et al.*, Science **298**, 587 (2002)] is based on a localized hot-spot effect induced by a near-field coaxial applicator. The microwave drill melts the nonmetallic material locally and penetrates mechanically into it to shape the hole. This paper presents a theoretical analysis of the thermal-runaway effect induced in front of the microwave drill. The model couples the Maxwell's and heat equations including the material's temperature-dependent properties. A finite-difference time-domain algorithm is applied in a two-time-scale numerical model. The simulation is demonstrated for mullite, and benchmarked in simplified cases. The results show a temperature rise of $\sim 10^3$ K/s up to 1300 K within a hot spot confined to a ~4-mm width (~0.1 wavelength). The input-port response to this near-field effect is modeled by equivalent time-varying lumped-circuit elements. Besides the physical insight, this theoretical study provides computational tools for design and analysis of microwave drills and for their real-time monitoring and adaptive impedance matching. © *2004 American Institute of Physics*.
[DOI: 10.1063/1.1836011]

I. INTRODUCTION

Thermal-runaway and hot-spot effects may occur accidentally in various volumetric microwave-heating processes.[1–6] Materials susceptible to these effects are characterized by particular temperature-dependent properties, such as a tendency of the dielectric loss to increase or of the thermal conductivity to decrease as the temperature rises. The microwave-power absorption tends to concentrate into a confined region evolving rapidly as a hot spot. In this local self-enhanced coupling process (analogous to a positive nonlinear feedback), the temperature rise is accelerated locally up to the melting point. This thermal-runaway effect may cause severe damages in microwave-heating processes that require uniformity, such as sintering or drying.[7,8] In this study, on the contrary, these thermal-runaway and hot-spot phenomena are considered advantageous for local heating and melting applications.

The microwave-drill concept[9] utilizes the thermal-runaway effect intentionally in order to drill into hard nonmetallic materials. A principle scheme of the microwave-drill applicator is illustrated in Fig. 1 (without the microwave source and the matching components). The microwave drill concentrates the radiation energy in the near field within the material, and generates a small hot spot there, much smaller than the microwave wavelength itself. In a thermal-runaway process, the material becomes soften or molten inside the bound hot spot. The center electrode is then inserted into the soft hot spot to form the hole.

The experimental results presented in Refs. 9–13 demonstrate the microwave-drilling effectiveness in various nonmetallic materials, including concrete, silicate minerals, silicon, glasses, and ceramics. The holes' diameters range from 0.5 mm in glass to 12 mm in concrete. The microwave-drilling effect is attained by concentrating the microwave power, typically to $\sim 10^2$ W/mm^2, within seconds. The microwave drill enables a distinction between different materials, and particularly between dielectrics and metals. For instance, the microwave drill can make holes and grooves in dielectric coatings with no damage to the underlying metallic substrate, as demonstrated for zirconia-based thermal-barrier coatings (>1500 °C melting temperature).[13]

This paper presents a theoretical analysis of the

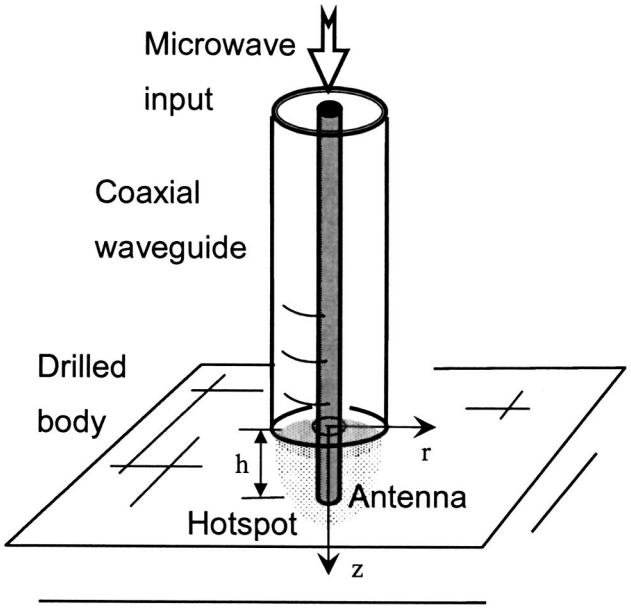

FIG. 1. A simplified scheme of the microwave-drill applicator consisting of a coaxial waveguide ended by a center-electrode "concentrator." The latter acts as a near-field monopole antenna (h) radiating the microwave energy into the hot spot excited in the drilling process. The center electrode is then inserted, mechanically, into the soften material to form the hole.

[a]Author to whom correspondence should be addressed; FAX: +972 3640 8048; electronic mail: jerby@eng.tau.ac.il

microwave-drill thermal-runaway process using a finite-difference time-domain (FDTD) model.[14,15] The analysis shows the governing factors of the localized-heating effect, the temperature profile around the center electrode, and the thermal-runaway process evolved in the near field. The input impedance of the microwave drill is modeled by equivalent time-varying lumped-circuit elements. Beside microwave drills, this analysis might be relevant as well to other local-heating and melting processes utilizing monopole microwave applicators in the near field.

II. THEORETICAL MODEL

The analysis of the microwave-drill mechanism couples the electromagnetic (EM) waves and their consequent thermal effects.[14,15] The EM waves emitted by the microwave monopole antenna and the power absorbed by the material are described by the Maxwell's equations for a lossy medium. For the cylindrical symmetry illustrated in Fig. 1, these equations are written in the form

$$\frac{\partial E_r}{\partial t} = -\frac{1}{\varepsilon_0 \varepsilon'}\left(\frac{\partial H_\varphi}{\partial z} + \sigma_d E_r\right), \tag{1a}$$

$$\frac{\partial E_z}{\partial t} = \frac{1}{\varepsilon_0 \varepsilon'}\left[\frac{1}{r}\frac{\partial}{\partial r}(rH_\varphi) - \sigma_d E_z\right], \tag{1b}$$

$$\frac{\partial H_\varphi}{\partial t} = \frac{1}{\mu_0}\left(\frac{\partial E_z}{\partial r} - \frac{\partial E_r}{\partial z}\right), \tag{1c}$$

where E_r and E_z are the radial and longitudinal electric-field components, respectively, H_φ is the azimuthal magnetic-field component, $\sigma_d = \omega_0 \varepsilon_0 \varepsilon''$ is the material's conductivity component associated with the dielectric loss, and $\varepsilon = \varepsilon_0(\varepsilon' - j\varepsilon'')$ is the complex dielectric coefficient. The absorbed power density is found, approximately, by

$$P_d = \omega_0 \varepsilon_0 \varepsilon'' \langle |\mathbf{E}|^2 \rangle, \tag{2}$$

where $\langle \cdots \rangle$ denotes a local root-mean-square (rms) time average.

The heat equation[16] is employed to find the local temperature profile excited by the absorbed microwave energy. The heat equation is rewritten in this case in the form

$$\rho_m c_m \frac{\partial T}{\partial t} = k_t\left[\frac{1}{r}\frac{\partial}{\partial r}\left(r\frac{\partial T}{\partial r}\right) + \frac{\partial^2 T}{\partial z^2}\right] + \frac{dk_t}{dT}\left[\left(\frac{\partial T}{\partial r}\right)^2 + \left(\frac{\partial T}{\partial z}\right)^2\right] + P_d, \tag{3}$$

where ρ_m, c_m, and k_t are the material's density, specific heat, and thermal conductivity, respectively, and T is the time-varying temperature profile. The temperature dependencies of the medium properties [i.e., $\rho_m(T)$, $c_m(T)$, and $k_t(T)$] are incorporated in this analysis as given in the material's data. The additional nonlinear term in the right-hand side of Eq. (3) is attributed to the temperature dependence of $k_t(T)$ and to its consequent spatial variation. As an example, the temperature-dependent dielectric and thermal properties of mullite are shown in Fig. 2, as given in Ref. 17. These are used in Sec. III to demonstrate the microwave-drill thermal-runaway effect in mullite. The variation of the material properties due to the local heating gives rise to a further increase in the local temperature.

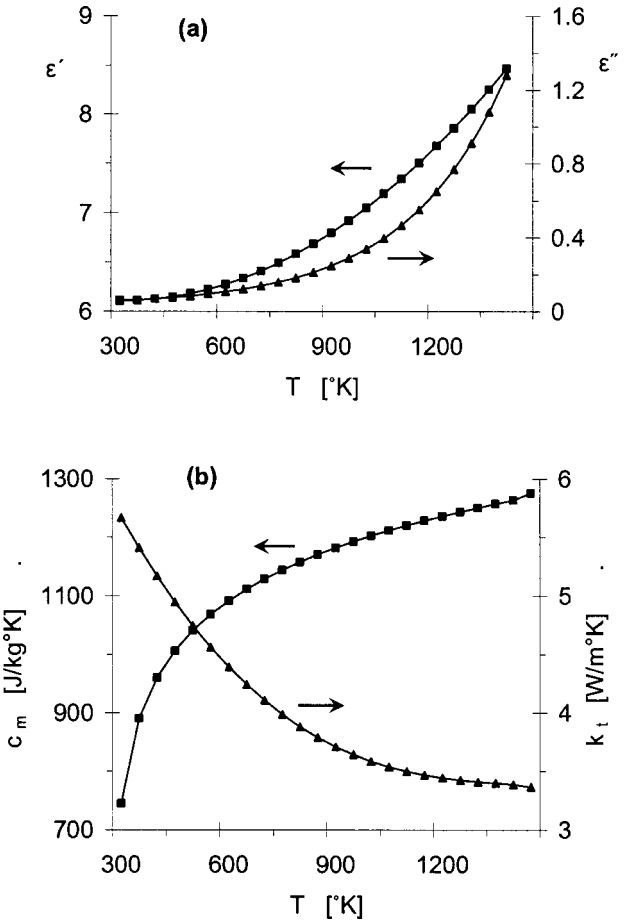

FIG. 2. The temperature-dependent properties of mullite (Ref. 17), (a) the real and imaginary parts of the dielectric permittivity, and (b) the specific heat and thermal conductivity.

This study uses a coupled thermal-EM algorithm consisting of two numerical solvers, one for the EM-wave Eqs. (1) and (2), and the other for the heat Eq. (3).[14,15] The time scale of the thermal effects is much longer than that of the EM waves, typically by a factor of $\sim 10^6$ or more (the EM wave propagates in few nanoseconds across this system). Hence, a two-time-scale approach is adopted to simplify the solution of the coupled equation set (1)–(3). The EM-wave propagation is computed in a relatively short period within each computation cycle of the thermal solver. The material properties are assumed to be stationary during these short periods of EM computations. The resulting absorbed power provides an input for the thermal solver (3). The local temperature and the material's parameters are updated in each computation cycle of the thermal solver. The temperature may increase up to the melting point. Phase-transition effects (melting and evaporation) are not included in the present model.

The numerical solution is performed by the FDTD method.[18–20] Starting from the given geometry and initial conditions, the EM solver computes the magnetic-field component (1c) first, and then uses the result for the solution of the electric-field components (1a) and (1b). Then, the EM

power absorption (2) is calculated to provide the generating power source for the solution of the heat equation (3). The local power absorbed depends on the dielectric-coefficient values, which depend, in turn, on the temperature. The dielectric coefficients are updated in each computation cycle, in each cell of the discrete FDTD mesh, taking into account the actual local temperature. In the discrete FDTD notation, Eq. (1b), for instance, attains the following form:

$$E^{n+1}_{z(i,j+1/2)} = \frac{1}{1+(\varepsilon''/2\varepsilon')\omega\Delta t}\left\{[1-(\varepsilon''/2\varepsilon')\omega\Delta t]E^{n}_{z(i,j+1/2)} + \frac{1}{\varepsilon_0\varepsilon'}\frac{\Delta t}{r_{(i,j+1/2)}\Delta r}[r_{(i+1/2,j+1/2)}H^{n+1/2}_{\varphi(i+1/2,j+1/2)} - r_{(i-1/2,j+1/2)}H^{n+1/2}_{\varphi(i-1/2,j+1/2)}]\right\}, \tag{4}$$

where Δt and n are the time step size and index, respectively, i and j are the radial and axial indices, respectively, of the mesh, and Δr and Δz are their corresponding step sizes. The local power density absorbed P_d (2) is computed as the input for the thermal solver at the center of each discrete cell (i.e., at the temperature node). The electric-field rms values at these nodes are found by interpolations. The discrete FDTD heat Eq. (3) is written in the form

$$T^{n+1}_{(i,j)} = T^{n}_{(i,j)} + \alpha\frac{k_t}{c_m\rho_m}\Delta t\left\{\frac{1}{\Delta r^2}\left[T^{n}_{(i+1,j)} - 2T^{n}_{(i,j)} + T^{n}_{(i-1,j)} + \frac{1}{(i-0.5)}(T^{n}_{(i+1,j)} - T^{n}_{(i,j)})\right] + \frac{1}{\Delta z^2}[T^{n}_{(i,j+1)} - 2T^{n}_{(i,j)} + T^{n}_{(i,j-1)}] + \frac{1}{k_t}P^{n}_{d(i,j)}\right\} + \frac{\alpha\Delta t}{c_m\rho_m}\left\{\frac{1}{\Delta r^2}[k^{n}_{t(i+1,j)} - k^{n}_{t(i,j)}][T^{n}_{(i+1,j)} - T^{n}_{(i,j)}] + \frac{1}{\Delta z^2}[k^{n}_{t(i,j+1)} - k^{n}_{t(i,j)}][T^{n}_{(i,j+1)} - T^{n}_{(i,j)}]\right\}, \tag{5}$$

where $\alpha = \tau_{\mathrm{Heat}}/\tau_{\mathrm{EM}}$ is the ratio between the computation periods of the heat and the EM equations in each cycle ($\alpha \sim 10^6$ here). Unless otherwise noted, ε', ε'', ρ_m, c_m, and k_t get their actual values in Eqs. (4) and (5) at each i, j node.

The microwave-drill workload dissipates heat by (a) convection through the surface boundaries, (b) radiation from the surface near the concentrator, and (c) conduction by the center electrode. The heat flux dissipated by convection is found by $q_{\mathrm{cond}} = h_f(T - T_a)$, where h_f is the convective heat-transfer coefficient and T_a is the ambient temperature. The heat (blackbody) radiation is given by $q_{\mathrm{Rad}} = \sigma\varepsilon_s(T^4 - T_a^4)$ where σ is the Stephan–Boltzmann constant and ε_s is the surface emissivity. Both components of heat-convection and radiation losses are subtracted from the $P^n_{d(i,j)}$ term in Eq. (5) in the corresponding boundary cells. The EM boundary conditions can be chosen as either ideal metallic or absorbing boundary conditions.

The EM waves propagating along the coaxial line feeding the microwave drill (Fig. 1) are computed as well. The results combine essentially the forward and reflected waves, whereas the reflections are caused by the impedance mismatch of the microwave-drill load. The resulting standing-wave pattern in the coaxial line enables us to find the time-varying reflection coefficient, $\Gamma_D(t)$. Given the characteristic impedance of the coaxial waveguide, Z_c, the time-varying load impedance of the microwave drill, $Z_D(t)$, is found by

$$Z_D(t) = Z_c\frac{1+\Gamma_D(t)}{1-\Gamma_D(t)}, \tag{6}$$

where $Z_c = (2\pi)^{-1}Z_0\ln(b/a)$ is the characteristic impedance of the coaxial line feeding the microwave drill, $Z_0 = \sqrt{\mu_0/\varepsilon_0}$ is the free-space impedance, and a and b are the inner and outer radii of the coaxial structure. The equivalent load impedance of the microwave drill is presented in the transmission-line equivalent model shown in Fig. 3, decomposed to real and imaginary components (R_D and X_D, respectively) in the form

$$Z_D = R_D + jX_D = R_{\mathrm{Heat}} + R_{\mathrm{Rad}} + j\omega L + \frac{1}{j\omega C}, \tag{7}$$

where R_{Heat} denotes the effective power absorbed as heat in the hot-spot region, and R_{Rad} stands for the ineffective power component radiated outside the drilling spot. The reactive elements L and C represent the inductive and capacitive stored energies, respectively, in the microwave-drill near-field region.

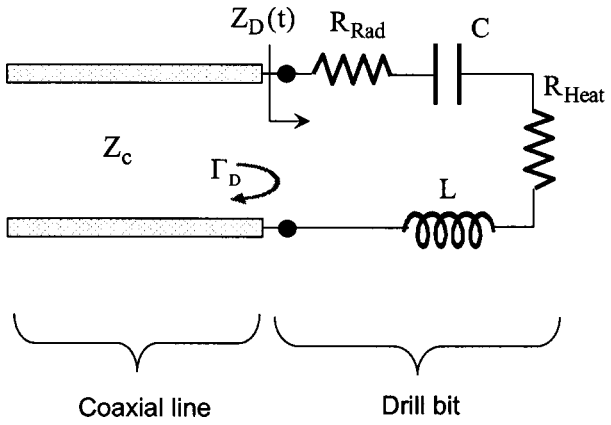

FIG. 3. An equivalent circuit of the microwave drill. The interaction region within the drilled material is represented by an equivalent lumped circuit with time-varying elements, depending on the thermal-runaway process evolution.

The equivalent circuit components (7) vary with time as the temperature distribution is evolved during the microwave-drilling process. The microwave power reflection is proportional to $|\Gamma_D(t)|^2$, thus an adaptive impedance-matching mechanism might be needed in practice in order to optimize the microwave-drilling efficiency.

As benchmarks for the FDTD simulation, its results are compared in simplified cases (e.g., uniform or constant material properties) with an analytical EM model and a commercial simulation code. The analytical model of a monopole antenna in a lossy uniform medium was derived from Refs. 21 and 22 assuming a sine current distribution along the antenna. Using the Poynting theorem, the heating and radiated power components and the stored (reactive) energy around the monopole antenna were found. The resulting approximations for the equivalent impedance components (7) are presented in the Appendix. The FDTD EM solver was benchmarked also with the commercial ANSOFT-HFSS code (Version 9).

Using the computational tools presented above, Sec. III presents the analyses of the microwave-drill heating process. The evolution of the temperature profile from a uniform distribution to a localized hot spot is simulated, and the corresponding microwave load impedance is characterized.

III. ANALYSIS

The microwave-drill mechanism and its near-field thermal-runaway process are simulated in this section for mullite. This material is chosen here as a typical example for ceramics and silicates with similar properties. The analysis employs the temperature-dependent properties shown in Fig. 2.[17] The other parameters are taken here as $\rho_m = 2500\ \mathrm{kg/m^3}$, $\varepsilon_s = 1$, and $h_f = 5\ \mathrm{W/m^2\,K}$. As a polycrystalline ceramic, the mullite's temperature-dependent parameters may vary significantly from one batch to another. Hence, the following analysis shall be regarded as an illustrative demonstration of the physical process, rather than a precise quantitative prediction for mullite in general.

The dimensions of the coaxial waveguide (Fig. 1) are chosen as 2- and 10-mm inner and outer diameters, respectively, and an 80-mm length. The radial dimensions correspond to a characteristic impedance of $Z_c \approx 100\ \Omega$, and the length is $\sim 2/3$ wavelength at 2.45 GHz. Unless otherwise noted, the effective input microwave power in the following analysis is 800 W and the ambient (and initial) temperature is $T_a = 300$ K.

The temperature rise in front of the microwave drill is presented in Fig. 4(a) for 600-W and 800-W effective input powers. The simulation results show different heating rates for the two different input powers. Furthermore, the thermal-runaway effect is evolved only for the 800-W input; as the temperature exceeds ~900 K, the rate of the further temperature increase is accelerated from $\sim 2\times 10^2$ K/s to $\sim 1.2\times 10^3$ K/s within ~2 s. In the lower 600-W microwave power, the slower temperature increase does not attain the thermal-runaway turning point in these conditions (similar thresholds have been observed in microwave-drilling experiments in various conditions[23]). Figure 4(b) shows the hot-spot width as the full width at half maximum (FWHM) of the temperature profile. The ~4.5-mm width corresponds to a ~0.1 wavelength. The near-field rapid temperature increase is associated with a further (relative) confinement of the hot spot, as seen in the 800-W curve in Fig. 4(b). This tendency to concentrate the energy within a confined hot spot characterizes the thermal-runaway phenomenon.

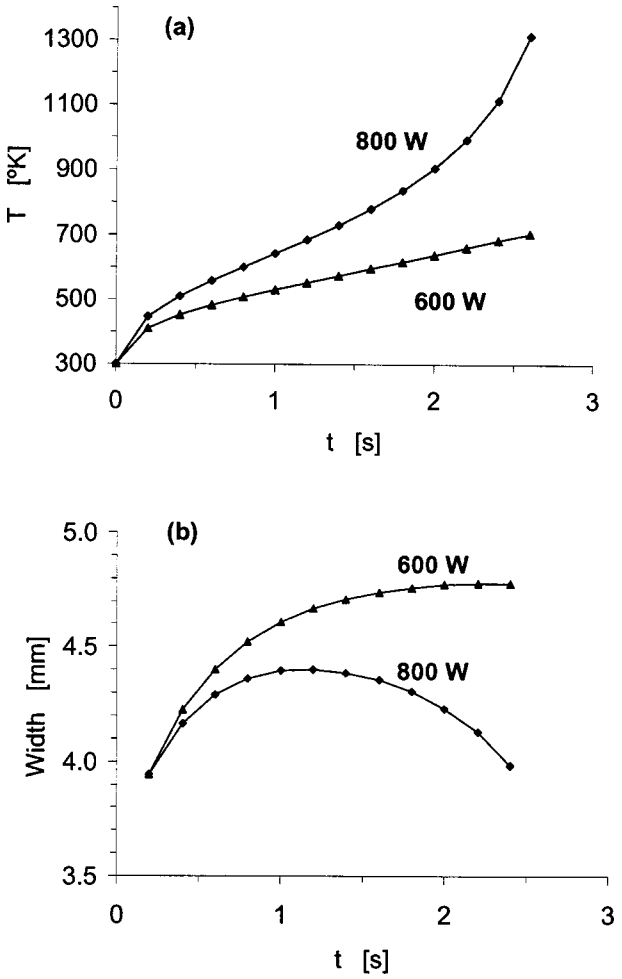

FIG. 4. The hot-spot buildups vs time in front of the microwave-drill center-electrode computed for 800-W (♦) and 600-W (▲) effective input powers. (a) The temperature evolved exhibits the thermal-runaway effect at 800 W. (b) The temperature profile width [i.e., full width half maximum (FWHM)] shows the hot-spot confinement in the thermal-runaway process.

The temperature profile evolved in the microwave-drill's near field is shown in Fig. 5(a). In this example, the center electrode is inserted to a 5-mm depth into the mullite bulk. The simulation result, after 2.6 s of an 800-W radiation, demonstrates the concentration of the high-temperature region in front of the center electrode. The corresponding profiles of the radial and axial electric-field components (E_r, E_z) are displayed in Figs. 5(b) and 5(c), respectively. The maximum electric-field strength in the hot spot is $|\mathbf{E}| \sim 3\times 10^5$ V/m, about three times higher than the maximum radial electric field at the interface with the coaxial waveguide. The axial electric-field component E_z is the major cause of the hot spot localized in front of the center electrode; hence it is essential for the proper microwave-drill operation.

The impact of the temperature-dependent material's

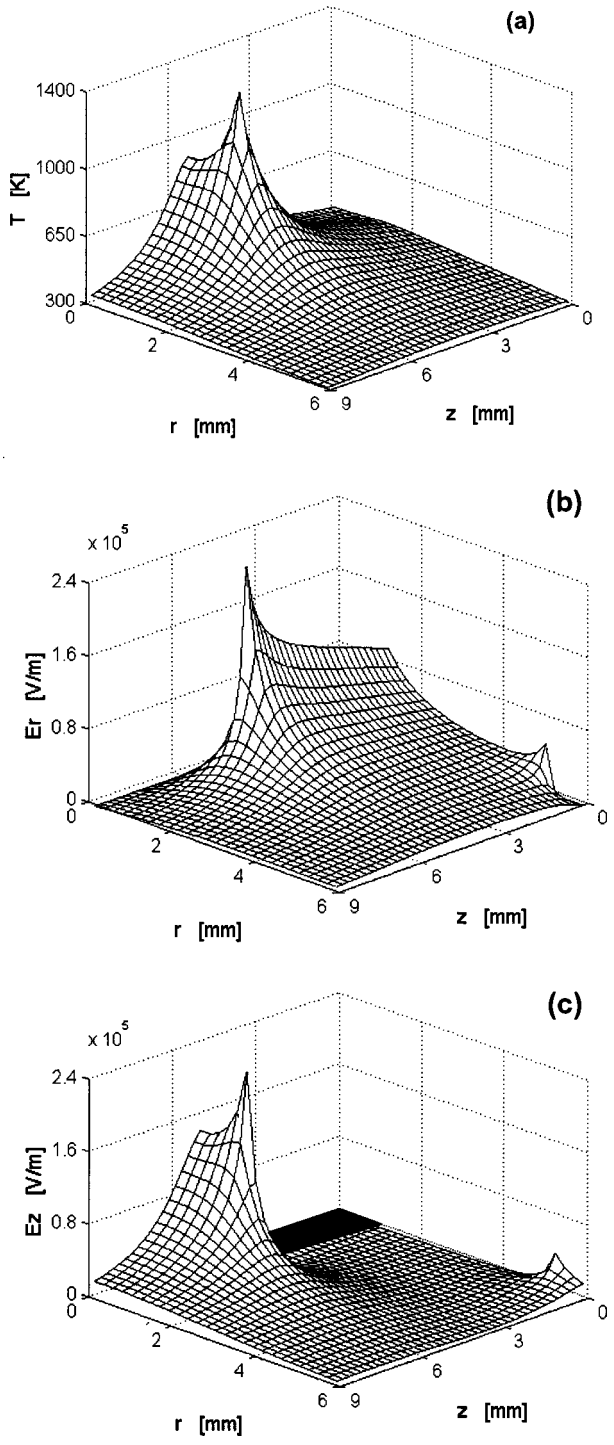

FIG. 5. Simulation results of the temperature and the field spatial distributions in mullite. The microwave-drill center electrode represented by the black area in (c) is inserted to $h=5$ mm. The temperature distribution (a) and the corresponding radial (b) and axial (c) electric-field components are shown for an 800-W radiation power in 2.6 s.

properties on the thermal-runaway evolution is demonstrated by four imaginary materials identical to mullite except that one parameter in each material is kept (numerically) constant in its room-temperature value. Figure 6 shows traces of the temperature evolution in these degenerated "materials" in a comparison to mullite with all temperature-dependent parameters (Fig. 2). The results show the positive contribution of $\varepsilon''(T)$ in real mullite to the thermal-runaway evolution,

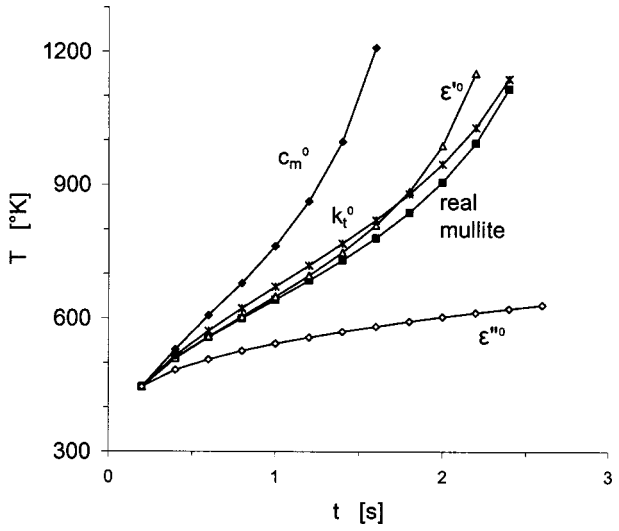

FIG. 6. The effects of the material properties' dependence on temperature, demonstrated for artificial examples of imaginary mullitelike materials compared with real mullite. In each curve the parameter noted (e.g., c_m^0) is kept numerically constant, in its room-temperature value, whereas the other parameters are taken as shown in Fig. 2 (the curves' legend is ◆ $c_m=c_m^0$, △ $\varepsilon'=\varepsilon'^0$, × $k_t=k_t^0$, ■ real mullite, and ◇ $\varepsilon''=\varepsilon''^0$). The room-temperature values are denoted c_m^0, ε'^0, k_t^0, and ε''^0 for the corresponding parameters. The effective input power is 800 W.

whereas the real $c_m(T)$ seems to play an impeding role in this respect. The effects of $\varepsilon'(T)$ and $k_t(T)$ are less significant [note that the decreasing effect of $k_t(T)$ is reduced by the second (nonlinear) term in the right-hand side of Eq. (3)]. These results coincide with our intuitive physical insight and with the roles of these parameters in Eqs. (3) and (4). Hence, the temperature rise is accelerated as the dielectric loss tangent ($\varepsilon''/\varepsilon'$) increases, or as the specific heat (c_m) decreases with temperature.

The sweep in the microwave-drill load impedance due to its center-electrode penetration into a varying depth h is presented in Figs. 7(a) and 7(b) for the real and imaginary parts, respectively. The FDTD results are benchmarked here with results obtained by the HFSS code and by the analytical model (Appendix) for a uniform temperature (300 K) profile. The agreement in this simplified case is satisfying (note that the analytical model assumes a coaxial-waveguide outer radius much smaller than the monopole-antenna's length, hence its imaginary part deviates at $h<6$ mm). The center-electrode penetration depth for which $X_D=0$ ($h\cong 11$ mm in this case) is a resonance length of the monopole antenna. The microwave-drill load impedance is either capacitive ($X_D<0$) or inductive ($X_D>0$) for shorter or longer penetration depths, respectively. The microwave-drill resistance at resonance ($R_D\cong 14\ \Omega$ at $h\cong 11$ mm) is considerably smaller than the coaxial-line characteristic impedance ($Z_c\approx 100\ \Omega$); hence a careful impedance matching is needed. The sweep in R_D (5–35 Ω) due to the center electrode varying penetration depth may require an adaptive impedance-matching mechanism in order to attain an optimal efficiency during the entire microwave-drilling process (the assumption of fixed effective input power in this analysis takes into account such an adaptive impedance matching).

The rapid temperature increase due to the thermal-

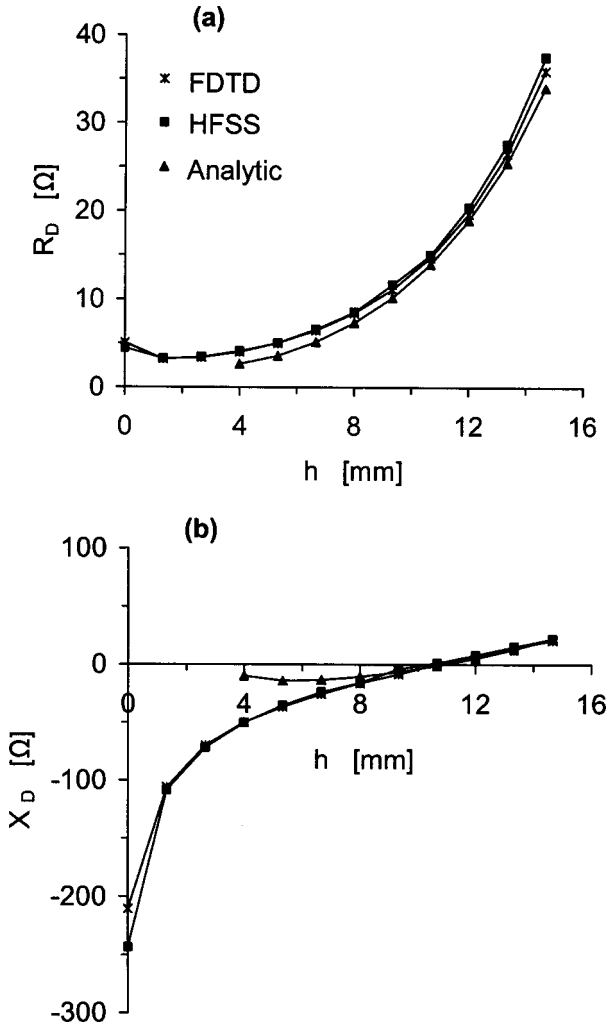

FIG. 7. The real (a) and imaginary (b) components of the microwave-drill impedance vs the center-electrode depth (h) in mullite. The FDTD simulation (■) is benchmarked at a uniform temperature (300 K) with the HFSS code (×) and the analytical model (▲).

runaway effect occurs locally near the coaxial-line open end. As it varies the material's properties there, it may change as well the loading impedance of the microwave drill (toward the generator) during the heating process. The resistive components of the microwave-drill equivalent impedance, denoted R_{Heat} and R_{Rad} in Eq. (7), are shown in Fig. 8 for a 2-mm fixed insertion depth in mullite (presented in Fig. 2). The distinction between R_{Heat} and R_{Rad} reveals the actual ratio between the effective power absorbed (as heat) and the ineffective radiation losses in the microwave-drill operation. As the hot spot evolves, the effective power component tends to increase; hence more energy is absorbed and transformed to heat. This effect though, of impedance variation due to the thermal runaway at a fixed insertion depth, is less significant than that caused by the varying insertion depth, as shown in Figs. 7(a) and 7(b). The actual microwave-drill operation[9–13] combines both causes of the impedance variation.

The reflection coefficient Γ_D variation with respect to the electrode insertion depth is depicted in Fig. 9. The two curves show the extreme cases of 300 K and 1300 K uniform temperatures for an 800-W effective input power. The actual reflection coefficient varies as the nonuniform temperature evolves from the upper curve toward the lower curve. The reflection coefficient Γ_D decreases as the insertion depth increases, or as the temperature increases. Hence, as the microwave drill proceeds, it tends to improve its impedance matching to the coaxial line (partly because of the radiation-loss increase). This pseudo-self-matching effect was observed in our preliminary microwave-drill experiments as well.

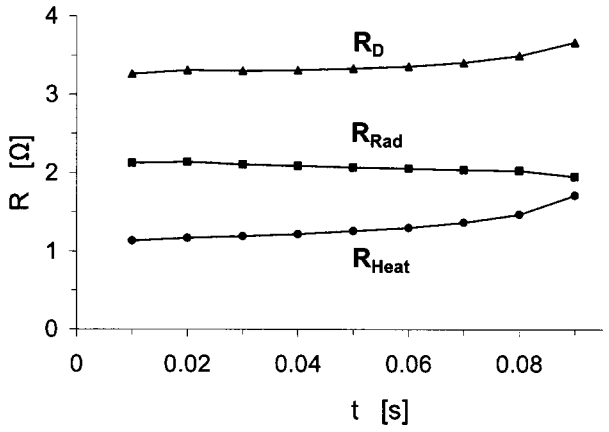

FIG. 8. The microwave-drill equivalent resistance vs time for mullite's parameters (given in Fig. 2). The distinction between R_{Heat} and R_{Rad} shows the effective and loss power components, respectively, in the microwave-drill operation in a fixed $h=2$ mm insertion depth (for an 800-W effective input power).

IV. DISCUSSION

The coupled thermal-electromagnetic FDTD model of the microwave drill was applied in this paper to analyze the

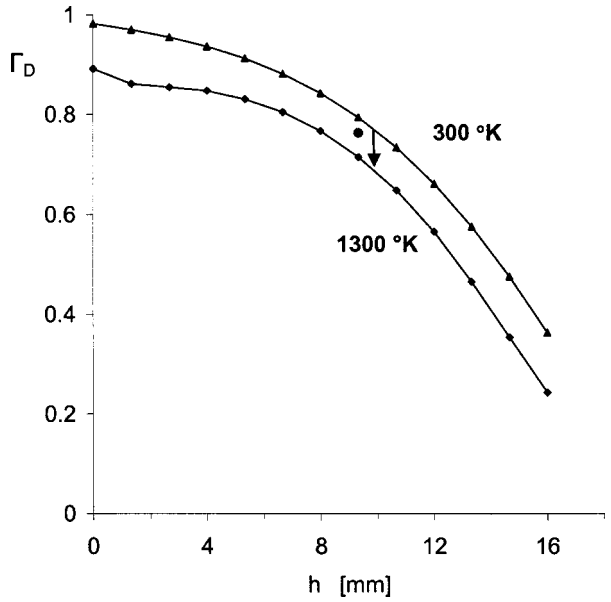

FIG. 9. The reflection coefficient at the microwave input port Γ_D vs the insertion depth of the center electrode h for mullite in uniform 300 K (▲) and 1300 K (♦) temperatures, at an 800-W effective input power. The reflection coefficient decreases as the temperature rises and as the electrode insertion is deepen. In the nonuniform heating phase, the actual $\Gamma_D(t)$ value is bound by these two curves; it begins on the upper curve (at room temperature) and proceeds down towards the lower curve while its local temperature increases, as shown, for example, by the FDTD simulation result (●).

microwave-drill phenomena in mullite (chosen for this analysis as a typical representative for ceramics and similar materials). The results show the hot-spot evolution in front of the microwave drill as a thermal-runaway process. The effects of the temperature-dependent material's properties on the heating process were identified. The variations in the microwave-drill's load impedance due to the varying insertion depth and the temperature evolution were found as well. This analysis provides an insight to the physical principles of the microwave-drill mechanism. In practice, this model will be used to design microwave drills for various materials, and for the analyses and monitoring of their operation.

Further studies related to this analysis are needed, including (a) numerical analyses of the microwave-drill operation in other materials (note that the temperature-dependent data, as given for mullite in Fig. 2, may not be completely available), (b) experimental studies of microwave drills in various materials and conditions in comparison with theory, and (c) a further development of a more comprehensive model describing the entire microwave-drill operation including phase-transition effects (melting and evaporation) simultaneously with the center-electrode penetration.

The microwave drill and its numerical simulation could be used together as an active measurement system in order to estimate missing parameters of the material's properties at high temperatures, by analyzing the reflected waves and the other measurable parameters. The microwave drill and its simulation could be further developed for other applications as well, including local heating and sensing, joining, pin insertion, and cutting in a variety of hard and soft materials.

APPENDIX: INPUT IMPEDANCE OF MONOPOLE ANTENNA IN LOSSY MEDIUM

This appendix presents approximated formulas for the load impedance of a monopole antenna inserted in a lossy medium. The model assumes a sinusoidal antenna current and a uniform medium.[21,22] Using the Poynting theorem and the induced-emf method adapted for a dissipative medium, the resistive and reactive impedance components (7) are found approximately as

$$R_{\mathrm{Rad}} \approx 10\frac{k}{\beta}L_{\mathrm{eq}}{}^{2}\left\{1+0.133\left[1-\left(\frac{\alpha}{\beta}\right)^{2}\right]L_{\mathrm{eq}}{}^{2} + 0.02\left[1-6\left(\frac{\alpha}{\beta}\right)^{2}+\left(\frac{\alpha}{\beta}\right)^{4}\right]L_{\mathrm{eq}}{}^{4}\right\}, \tag{A1}$$

$$R_{\mathrm{Heat}} = \frac{k}{\beta}\frac{K_a}{1+(\alpha/\beta)^2}\frac{A(1+B^2)+\dfrac{\alpha}{\beta}B(1-A^2)}{A^2+B^2}, \tag{A2}$$

$$X_D = \frac{k}{\beta}\frac{K_a}{1+(\alpha/\beta)^2}\frac{\dfrac{\alpha}{\beta}A(1+B^2)-B(1-A^2)}{A^2+B^2}, \tag{A3}$$

where $\alpha = k\sqrt{(\sqrt{1+x^2}-1)\varepsilon'/2}$ and $\beta = k\sqrt{(\sqrt{1+x^2}+1)\varepsilon'/2}$ are the decay factor and the wave number in the medium, respectively, $x=\tan\delta=\varepsilon''/\varepsilon'$ is the loss tangent, λ and $k=2\pi/\lambda$ are the free-space wavelength and wave number, respectively, and $\varepsilon=\varepsilon'-j\varepsilon''=\varepsilon'(1-j\tan\delta)$ is the complex dielectric permittivity of the medium. The antenna's equivalent length is $L_{\mathrm{eq}}\approx\beta h\{1+0.19/[\ln(h/a)-0.81]\}$, and $K_a=60[\ln(h/a)-1]$ is its "average" characteristic impedance in free space. The other parameters are $A=\tan h[(\alpha/\beta)L_{\mathrm{eq}}]$ and $B=\tan L_{\mathrm{eq}}$. The model assumes that the antenna's dimensions satisfy $h/a \gg 10$, $b/a<2$, and $L=\beta h \leqslant \pi/2$.

[1] G. Roussy, A. Bennani, and J. M. Thiebaut, J. Appl. Phys. **62**, 1167 (1987).
[2] G. A. Kriegsmann, J. Appl. Phys. **71**, 1960 (1992).
[3] P. E. Parris and V. M. Kenkre, Phys. Status Solidi B **200**, 39 (1997).
[4] G. A. Kriegsmann, IMA J. Appl. Math. **59**, 123 (1997).
[5] C. A. Vriezinga, J. Appl. Phys. **83**, 438 (1998).
[6] X. Wu, J. R. Thomas, and W. A. Davis, J. Appl. Phys. **92**, 3374 (2002).
[7] A. C. Metaxas, *Foundations of Electroheat—A Unified Approach* (Wiley, New York, 1996).
[8] J. Thuery, *Microwave: Industrial, Scientific, and Medical Applications* (Artech House, Boston, MA, 1992).
[9] E. Jerby, V. Dikhtyar, O. Aktushev, and U. Grosglick, Science **298**, 587 (2002).
[10] E. Jerby and V. Dikhtyar, *Drilling into Hard Non-conductive Materials by Localized Microwave Radiation*, Proceedings of the Eighth Ampere International Conference on Microwave and High-Frequency Heating, Bayreuth, Germany, 4–7 September 2001 (unpublished) (see in www.microwave-drill.org).
[11] E. Jerby, V. Dikhtyar, and O. Aktushev, Am. Ceram. Soc. Bull. **82**, 35 (2003).
[12] E. Jerby and V. Dikhtyar, Water Well j. 32 (2003).
[13] E. Jerby and A. M. Thompson, J. Am. Ceram. Soc. **87**, 308 (2004).
[14] Y. Alpert and E. Jerby, IEEE Trans. Plasma Sci. **27**, 555 (1999).
[15] U. Grosklick, V. Dikhtyar, and E. Jerby, European Symposium on Numerical Methods in Electromagnetics, JEE'02 Proceedings, Toulouse, France 6–8 March 2002 (unpublished).
[16] F. P. Incropera and D. P. Dewitt, *Fundamentals of Heat and Mass Transfer* (Wiley, New York, 1985).
[17] C. C. Goodson, M.Sc. thesis, Virginia Tech., 1997; see also X. Wu, Ph.D. thesis, Virginia Tech., 2002 (both in http://scholar.lib.vt.edu/theses).
[18] A. Taflove and S. C. Hagness, *Computational Electrodynamics* (Artech House, Boston, MA, 2000).
[19] L. Ma and D. L. Paul, IEEE Trans. Microwave Theory Tech. **43**, 2565 (1995).
[20] F. Torres and B. Jecko, IEEE Trans. Microwave Theory Tech. **45**, 108 (1997).
[21] R. W. P. King, C. W. Harrison, *Antennas and Waves: A Modern Approach* (M.I.T., Boston, MA, 1969).
[22] E. C. Jordan and K. G. Balmain, *Electromagnetic Waves and Radiating Systems*, 2nd ed. (Prentice-Hall, Englewood Cliffs, NJ, 1968).
[23] E. Jerby, O. Aktushev, V. Dikhtyar, O. Harpaz, and P. Livshits, *Microwave Drilling Overview (ceramics, glass, basalt)*, Proceedings of the Fourth World Congress on Microwaves and Radio-Frequency Applications, Austin, Texas, 7–11 November 2004 (unpublished).